Pure Appl. Geophys.

https://doi.org/10.1007/s00024-018-1898-6

Pure and Applied Geophysics

Suitability of Open-Ocean Instrumentation for Use in Near-Field Tsunami Early Warning Along Seismically Active Subduction Zones

Amy L. Williamson[1] and Andrew V. Newman[1]

Abstract—Over the past decade, the number of open-ocean gauges capable of parsing information about a passing tsunami has steadily increased, particularly through national cable networks and international buoyed efforts such as the Deep-ocean Assessment and Reporting of Tsunami (DART). This information is analyzed to disseminate tsunami warnings to affected regions. However, most current warnings that incorporate tsunami are directed at mid- and far-field localities. In this study, we analyze the region surrounding four seismically active subduction zones, Cascadia, Japan, Chile, and Java, for their potential to facilitate local tsunami early warning using such systems. We assess which locations currently have instrumentation in the right locations for direct tsunami observations with enough time to provide useful warning to the nearest affected coastline—and which are poorly suited for such systems. Our primary findings are that while some regions are ill-suited for this type of early warning, such as the coastlines of Chile, other localities, like Java, Indonesia, could incorporate direct tsunami observations into their hazard forecasts with enough lead time to be effective for coastal community emergency response. We take into account the effect of tsunami propagation with regard to shallow bathymetry on the fore-arc as well as the effect of earthquake source placement. While it is impossible to account for every type of off-shore tsunamigenic event in these locales, this study aims to characterize a typical large tsunamigenic event occurring in the shallow part of the megathrust as a guide in what is feasible with early tsunami warning.

Key words: Tsunami early warning, near-field, DART gauge, earthquakes.

1. Introduction

Many tsunami warnings stem form an evaluation of the seismic energy released from tsunami-generating earthquakes. Then, if available, additional data about the tsunami are incorporated to update mid and far-field tsunami warnings. While a seismic dataset is valuable for understanding the earthquake source dynamics, the relationship between the seismic energy determined earthquake magnitude and tsunami energy used for event warnings and forecasts is non-linear and poorly understood (Tang et al. 2012). Even with a well constrained seismically determined magnitude, the application to tsunami hazard is not always absolute. As highlighted in Titov et al. (2016a), the tsunami warnings issued for many recent earthquakes based on seismic evaluations did not accurately describe the oncoming wave. In the cases of the moment magnitude, M_w, 8.6 2005 Nias Island earthquake and the 2012 M_w 8.6 Sumatra earthquake, the tsunami threats were overestimated, in some cases leading to unnecessary and costly evacuations with little to no eventual damage related to the tsunami (Song 2007; Titov et al. 2016a). On the other hand, in the cases of the 2006 West Java earthquake (M_w 7.7), no official tsunami warning was issued and an eventual run-up of up to 21 m was recorded in Pangandaran (Okal 2015; Fritz et al. 2007). This earthquake, like the 2010 Mentawai Islands earthquake (M_w 7.8), was a 'tsunami earthquake' (Newman et al. 2011). Tsunami earthquakes oftentimes produce tsunami that are much larger than seismic models rapidly predict (Kanamori 1972; Kanamori and Kikuchi 1993; Newman and Okal 1998) with slip concentrated in the shallow megathrust environment (Polet and Kanamori 2000). While seismic evaluations of the tsunami are valuable—particularly in the near-field where tsunami landfall can be within tens of minutes, a direct measurement of the tsunami for forecasting purposes provides a

Electronic supplementary material The online version of this article (https://doi.org/10.1007/s00024-018-1898-6) contains supplementary material, which is available to authorized users.

[1] School of Earth and Atmospheric Sciences, Georgia Institute of Technology, 311 Ferst Drive, Atlanta, GA 30332, USA. E-mail: amy.williamson@gatech.edu

Published online: 15 May 2018

useful dataset for emergency management. Direct observations lessen the chance of a misestimate of the tsunami, which can be devastating for the near-field environments where the majority of tsunami victims are located (Titov et al. 2016b).

Unlike far-field warnings where source to arrival is on the scale of hours, near-field warnings need to be computed on a severely abbreviated timeframe. One potential aid is the travel time differential between the open-ocean and shallow coastal environments. A tsunami will propagate with a higher velocity in deep water than it will over the shallower continental shelf. This discrepancy was identified for use in far-field tsunami forecasts in Titov et al. (2005) where the placement of sensors in the central Pacific allowed for the computation of lead times between measurement and inundation for the Hawaiian coastal city of Hilo. The efficacy of real-time open-ocean measurements of tsunami generated from far-field sources for forecasts in Hilo was demonstrated through idealized placements of then test-phase tsunameters. Idealized placements allowed for measurement and processing of the oncoming wave prior to inundation at the city—but focused solely on distantly generated events. This study operates under a similar premise as the Titov et al. (2005) study, but with a focus on near-field, rather than far-field generated events over multiple regions where tsunameters could be placed.

After considerable attention on far-field inundation forecasts, near-field early warning is the latest frontier for tsunami warning systems (Song 2007; Titov et al. 2016b). Prior work has assessed the usage of coastal GPS and assimilation of Deep-Ocean Assessment and Reporting of Tsunami (DART) gauges for improved early warning by rapidly approximating tsunami energy (Titov et al. 2016a). With these prior works in mind, this paper analyzes the suitability for localized near-field tsunami warning systems incorporating direct open-ocean tsunami observations, like those measured by DART gauges. We focus on four seismically-active regions, highlighting unique characteristics to take into account for early warning systems including coastal morphology, subducting plate geometry, tsunami source-to-landfall travel times, and currently deployed instrumentation. The goal of this study is not to reformat current warning system operations, but to investigate the feasibility of open-ocean data incorporation.

The study is divided into the following sections. First we outline currently deployed open-ocean instrumentation and its use in tsunami warning systems. Second we provide our methodology and analysis of the feasibility for localized near-field early warning for our four study regions—Cascadia, Japan, Indonesia, and Chile. Third, we discuss the variability of certain model parameters used in tsunami early warning and how they affect our results.

2. *Data*

Open-ocean pressure sensors provide a clean dataset that directly records the passage of tsunami waves. Within the past decade, DART gauge data have been incorporated in real time for tsunami warnings in the United States (Titov et al. 2016b). Each gauge measures the pressure exerted on a seafloor sensor from the overlying water column, translating it to a water column height. Data from each gauge are transmitted to warning centers via satellite and are openly available in semi-real time, offering a direct observation of a passing tsunami that is incorporated into tsunami warning forecasts. The gauges monitor for not only seismically induced tsunamis (Wei et al. 2014), but also from non-seismic events such as landslide tsunamis and meteotsunamis. Currently, there is a globally distributed array of 60 DART gauges owned by a consortium of countries. Most currently deployed gauges sit far from potential tsunami sources. Newer DART 4G instruments, which are in test operations offshore Oregon and Chile, are capable of up to a 1 Hz sampling frequency (Rabinovich and Eblé 2015; Tang et al. 2016) and are deployed closer to the trench and potential tsunami sources.

It is important to note that DART gauges are not deployed with the goal of providing tsunami forecasts for the immediate near-field. Current station capabilities are tailored for mid- to far-field forecasting. Furthermore, DART gauges are not the only instruments available in the open-ocean for tsunami modeling. Cabled networks that include similar

pressure gauge technology exist in a few locations. We highlight the deployment and capabilities of these observatories in subsequent sections of this paper. While this paper investigates near-field warnings using any open-ocean tsunami data, we use the current distribution of DART as a reference point because of their ubiquity in tsunami modeling and global presence.

3. Methodology

In order to examine the tsunami lead time (between data acquisition and earliest tsunami landfall), we generate a series of trench-parallel synthetic seafloor displacements. For each event, we track the travel time of the crest of the leading wave to determine the difference in travel time towards the open-ocean versus the shoreline (shown in Fig. 1). The earliest arrival time of the tsunami at the shoreline is recorded and used to determine the open-ocean boundary of which a station must be placed in order to capture the first one-quarter of the leading wave prior to its coastal inundation. We then highlight zones inside this boundary where a station must be placed in order to record the tsunami with variable lead times. By combining the results of multiple sources along the strike of the subduction zone, we can generate a composite view for each of our four study regions, to analyze which parts of the subduction zone are ideal for early warning, and which regions inhibit such early forecasts.

The sea-surface displacement generated from each synthetic tsunami source is used as an initial condition for tsunami propagation. Each seafloor displacement is described as a two-dimensional concave surface defined by:

$$H = \frac{1}{4}\left(1 + \cos\left(\frac{\pi x}{L}\right)\right)\left(1 + \cos\left(\frac{\pi y}{L}\right)\right)$$

where L is the diameter of the source and H is the two-dimensional water column profile over a spatial domain governed by x and y (Hossen et al. 2015). We place each of our synthetic sources above the region where we expect the subducting slab to be at a depth of 15 km (Hayes et al. 2012). The reasons for this placement are (1) this depth typically considered the upper extent of the seismogenic zone that nucleates large earthquakes (Lay 2015); and (2) the shallow environment is close to what can be expected for dangerous tsunami earthquakes.

We model the propagating tsunami from each synthetic event over a regional spatial domain with a 1 arc minute bathymetry. We run each simulation using the Method of Splitting Tsunami (MOST) model, which solves the non-linear shallow water wave equations (Titov and González 1997) and is currently an operational tool at the NOAA Tsunami Warning Centers and at the NOAA Center for Tsunami Research.

An example of our analysis using a single synthetic source is shown in Fig. 1. The earliest landfall of the crest of the leading wave, 18 min after nucleation, is recorded for determining instrument warning zones. The simultaneous location of the tsunami's leading wave in open-ocean identifies the furthest extent of the near-field early warning capabilities, acting as a threshold for instrument placement. This threshold contour acts as a 0-min warning zone. The 0-min warning region means any station placed in this shaded region will be measured at about the same time as landfall for local events. Anything inside of this contour will register the tsunami before landfall; however, some areas will record the tsunami with a greater lead time than other areas. To calculate the lead times inside of this threshold for this synthetic event is fairly simple. The lead time for any location is equal to the coastal arrival time subtracted from the tsunami travel time. In Fig. 1, we highlight zones that have 5 and 10 min of lead time before coastal inundation. For each of the subsequent composite figures, we draw shaded regions of expected lead times from 0 min up to 20 min at 5-min increments, where possible.

It is extremely important to note that the location of our synthetic source has a role in the timing of the earliest inundation on land and this threshold of open-ocean detection. We pick our source location, as mentioned earlier, for its consideration as the 'edge' of the typical seismogenic zone. However, any event rupturing primarily up-dip of this synthetic event will have a longer time until inundation, and events rupturing primarily down-dip will have a quicker inundation. We stress this variability and uncertainty

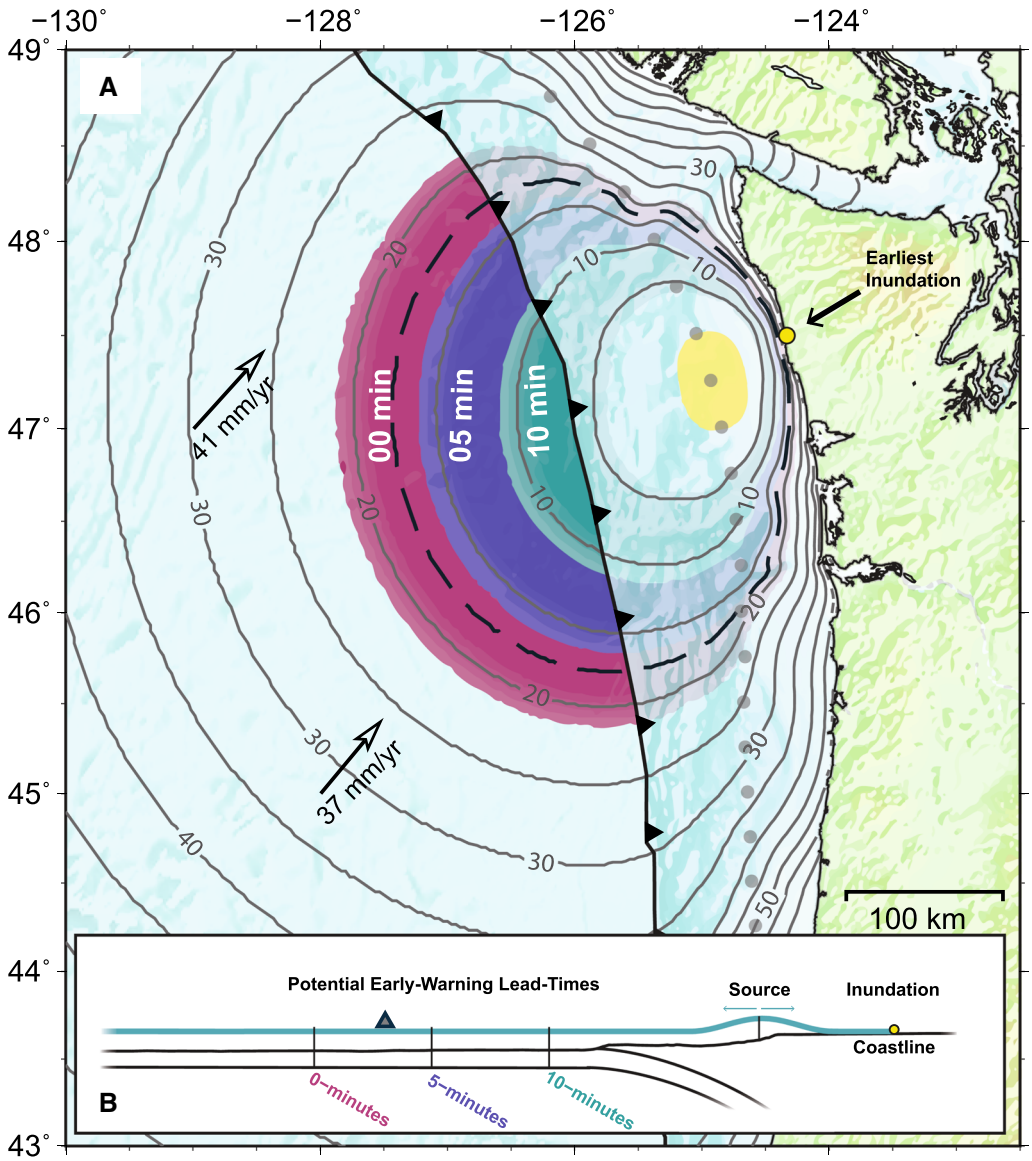

Figure 1

a Propagation of a single synthetic event to determine instrument zones for local early tsunami warning. The synthetic event's source is shown as the light-yellow polygon. The travel time, in minutes, of the crest of the leading wave from this source is plotted by the gray contours. The location of the earliest inundation (at 18 min) is marked with a yellow dot on the coastline. The location of the tsunami's leading wave at this time is outlined by the black dashed line. The magenta, navy, and aqua shaded regions on the subducting plate indicate 0-, 5-, and 10-min zones for possible instrument placement. The gray dots along strike of the trench shows the rest of the synthetic locations that will be combined in the composite image (Fig. 2). Arrows indicate the plate motion between the Juan de Fuca and North American plates using MORVEL-2010 motions (DeMets et al. 2010). **b** Cross-section schematic of the source, inundation, and warning zones for near-field tsunami early warning, generalizing the map shown in **a**

in source location by creating a 2.5-min window on either side of our lead time estimate, as a way to take into account slightly shallower and slightly deeper events. Therefore, each lead time estimate, as shown in Fig. 1, is displayed as a zone rather than a single line.

Figure 1 shows only a single-source solution to demonstrate the methodology, but each final

composite image is composed of multiple synthetic events. The spacing of each of these synthetic events is 15′ latitude and longitude in the trench-normal direction. At an equatorial site this amounts to one synthetic source about every 30 km along strike. This spacing allows for the characterization of each section of the subduction zone for its near-field warning capabilities from local offshore data. Regional early-warning images in subsequent figures combine many synthetic events into one composite. Each event's output is weighted equally, where the center of each lead time zone (treated as independent polygons) is assigned the value '1' and areas not in the warning zone are assigned a value of '0'. After all of the same lead time zones are combined via a simple summation into the composite and normalized; areas in each warning zone with a value lower than a threshold 0.1 are discarded. This acts as a filter to avoid the inclusion of spurious areas that do not overlap, or overlap little with neighboring events, due to either poorly resolved bathymetry or extremely fine scaled features, and to smooth small irregularities in lead times. After the composite for each warning zone is created, a final image merges each warning zone together, as shown in Figs. 2, 3, 4, and 5. We want to reiterate that the use of lead times is applicable for a local and trench-normal relationship between the offshore instrumentation, tsunami nucleation point, and nearby coast. A lead time of 10 min in Cascadia, for example, is drawn for an event's immediate surroundings and combined with neighboring events to show the general extent of that level of warning for any area, but should not be extended to assume that an instrument at the southernmost point of Cascadia can provide a 10-min warning for an event originating at the northernmost point for coastal communities also at the northernmost extent of the model-space.

4. Results

The results of five composite images for four near-field tsunami warning cases are explored. Each region is picked due to either unique megathrust geometries, coastal morphology, the threat of a future large event, or the preponderance of large tsunamigenic events in the past. We focus entirely on subduction zone megathrust environments because of their tsunamigenic potential due to megathrust earthquakes and current open-ocean tsunami instrumentation.

4.1. Cascadia

Attention has been focused on the Cascadia subduction zone in recent years in preparation for the possibility of a great tsunamigenic earthquake rupturing along the trench (Satake et al. 1996; Satake et al. 2003). The most recent large tsunami generated from the region occurred in 1700 A.D., supported from Japanese tsunami deposit records and tree ring analysis along the Pacific Northwest (Satake et al. 1996; Atwater 1992). Estimated sources of the 1700 tsunami have been modeled to compare with Japanese coastal records, supporting a claim that the earthquake which generated the tsunami ruptured over 1100 km of the megathrust with a magnitude close to 9.0 (Satake et al. 2003). While the megathrust remains seismically quiet, the region is known for frequent slow-slip events near the deeper portion of the subduction interface (Rogers and Dragert 2003). Currently, with land-based tools, it is unclear if the shallower portion of this interface is locked, or freely slipping, giving little guidance to the seismic hazard. There have been many recent studies on this matter, producing many models of a possible large megathrust event. These models aid in our understanding of possible hazards associated from the tsunami, such as inundation extent, as well as seismic characteristics, such as peak-ground-acceleration that could be expected on land (Witter et al. 2013; Melgar et al. 2016).

Building on the methodology example from Figs. 1, 2 shows the regional composite view of early warning for the Cascadia subduction zone in the Pacific Northwest. The young Juan de Fuca plate subducts underneath the North American plate at about 40 mm/year (DeMets et al. 2010). The offshore coastal region between the trench and coastline is fairly broad with distances that can exceed 100 km. The regional bathymetry includes a wide and broad continental shelf that extends far off the Oregon and Washington coastlines before tapering towards Vancouver Island. This composite solution merges the

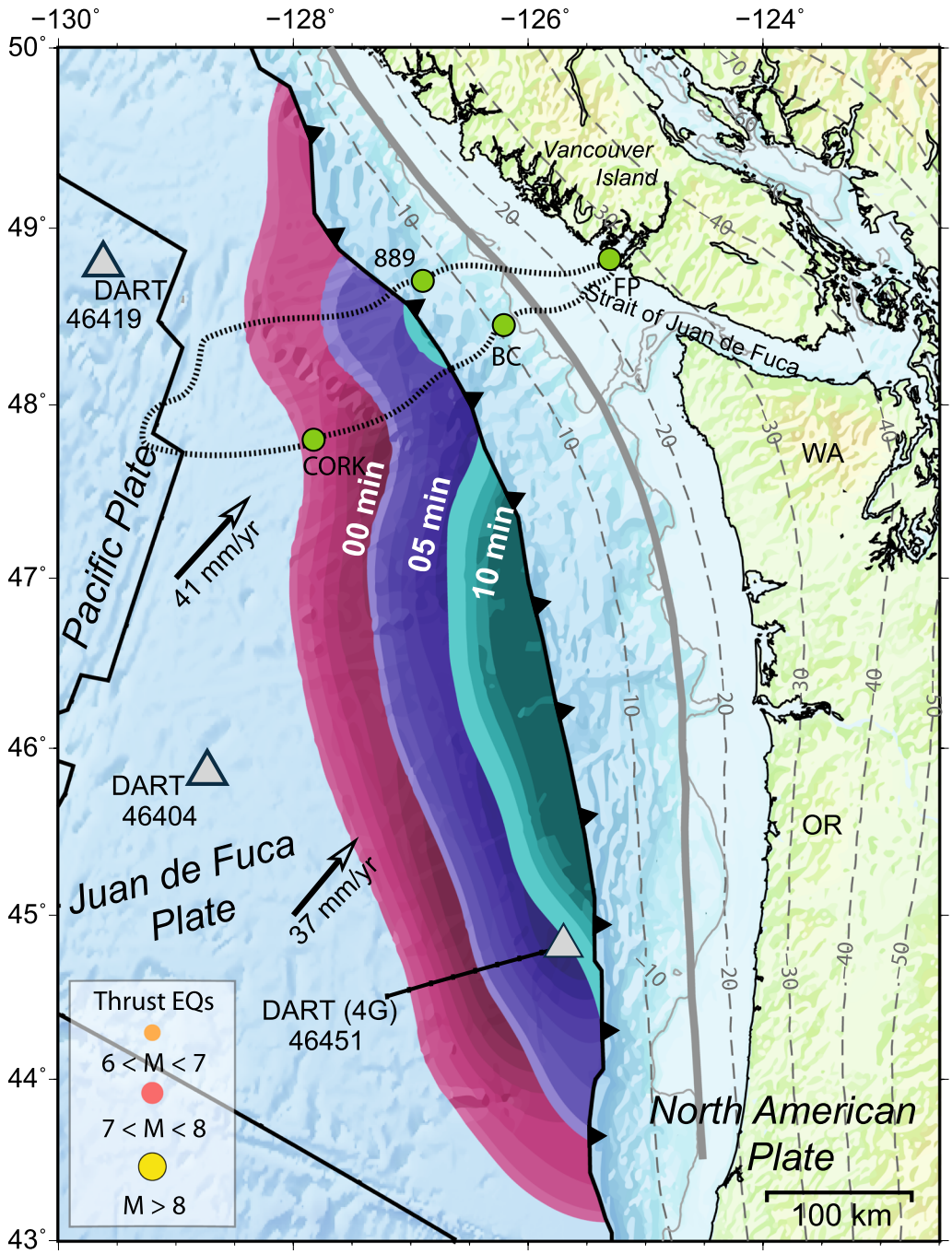

Figure 2

Composite view of Cascadia early warning zones. Magenta, navy, and aqua shading refers to 0 min, 5-min, and 10-min lead times, respectively. Arrows indicate the plate motion between the Juan de Fuca and North American plates using MORVEL-2010 motions (DeMets et al. 2010), gray triangles show approximate locations of DART gauges, and green dots indicate the location of NEPTUNE bottom pressure sensors used for tsunami studies. The thick, gray line that runs trench parallel shows the location of synthetic sources used in the composite. Unlike subsequent figures, there are no recorded earthquakes greater than M 6 with a thrust focal mechanism to display to illustrate seismicity around the megathrust

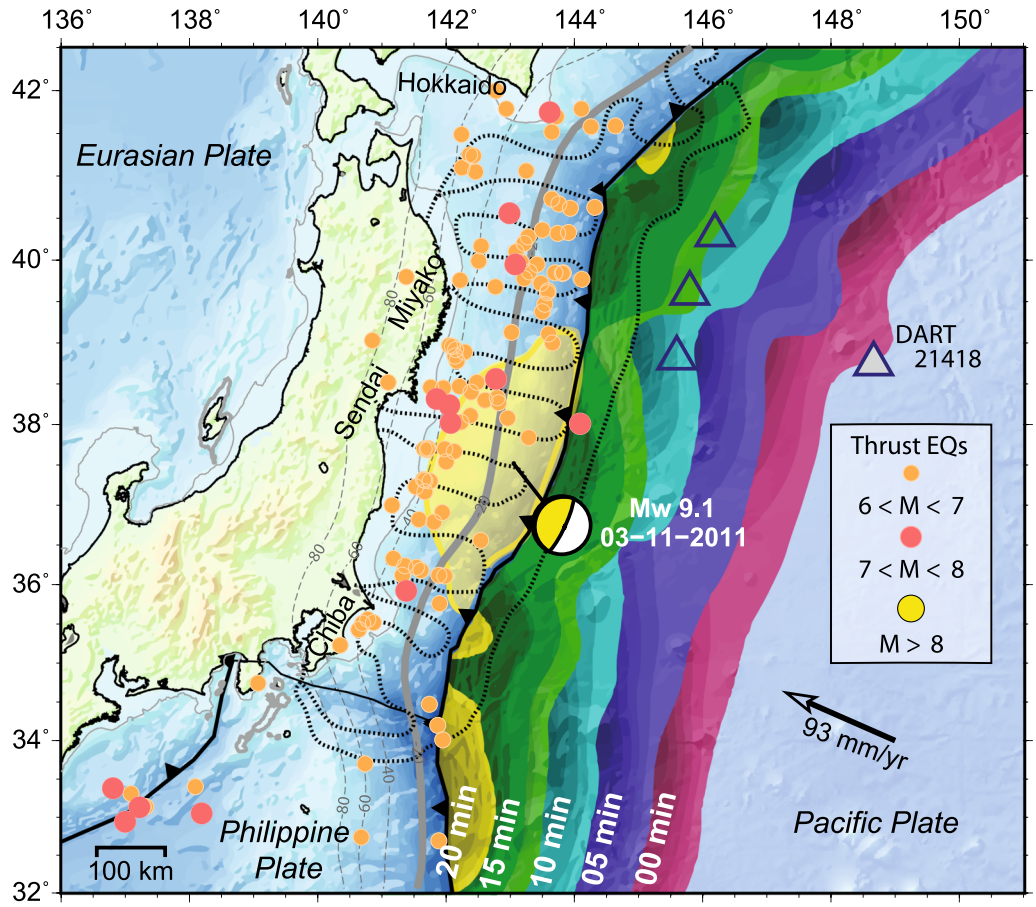

Figure 3

Composite view of northern Japan early warning zones. Magenta, navy, aqua, green, and yellow shading refers to 0 min, 5-min, 10-min, 15-min, and 20-min lead times, respectively. Arrows indicate the plate motion between the Pacific and Eurasian plates using MORVEL-2010 motions (DeMets et al. 2010) and gray triangles show approximate locations of DART gauges. The thick, gray line that runs trench parallel shows the location of synthetic sources used in the composite. Small dots indicate seismicity recorded in the Harvard CMT catalog over the past 25 years. Yellow shaded region is the approximate rupture extent of the 11 March 2011 Tohoku earthquake (Wei et al. 2014). Hollow triangles indicate DART gauges deployed following the 2011 Tohoku tsunami but have since been decommissioned. Black dashed line outlines the cabled S-NET array

warning zones from 22 synthetic trench-parallel events along the megathrust interface. The megathrust interface has a fairly shallow inferred dip, placing the synthetic event boundary close to the continental shelf. Each lead time zone (0-, 5- and 10-mins) highlighted in Fig. 2 is composed by first determining the warning zone on each individual model, as shown in Fig. 1 and then combining each zone together for a regional view.

The best zone for near-field deep-ocean instrumentation extends from 44.5° to 47.5°N where a 10-min lead time is possible for local events. To the south of this zone, land extends further along the interface, precluding shallow earthquakes from displacing enough of the water column be tsunamigenic. Additionally, the continental shelf's width tapers, locally affecting the wave velocity. To the north, the mouth of the Strait of Juan de Fuca inhibits the shoaling and slowing of the tsunami, leading to a quicker inundation at the opening of the strait. Further north along Vancouver Island, the ability to include near-field open ocean datasets declines as the distance to the coast diminishes. Outside of the 10-min warning, the 5-min zone extends further

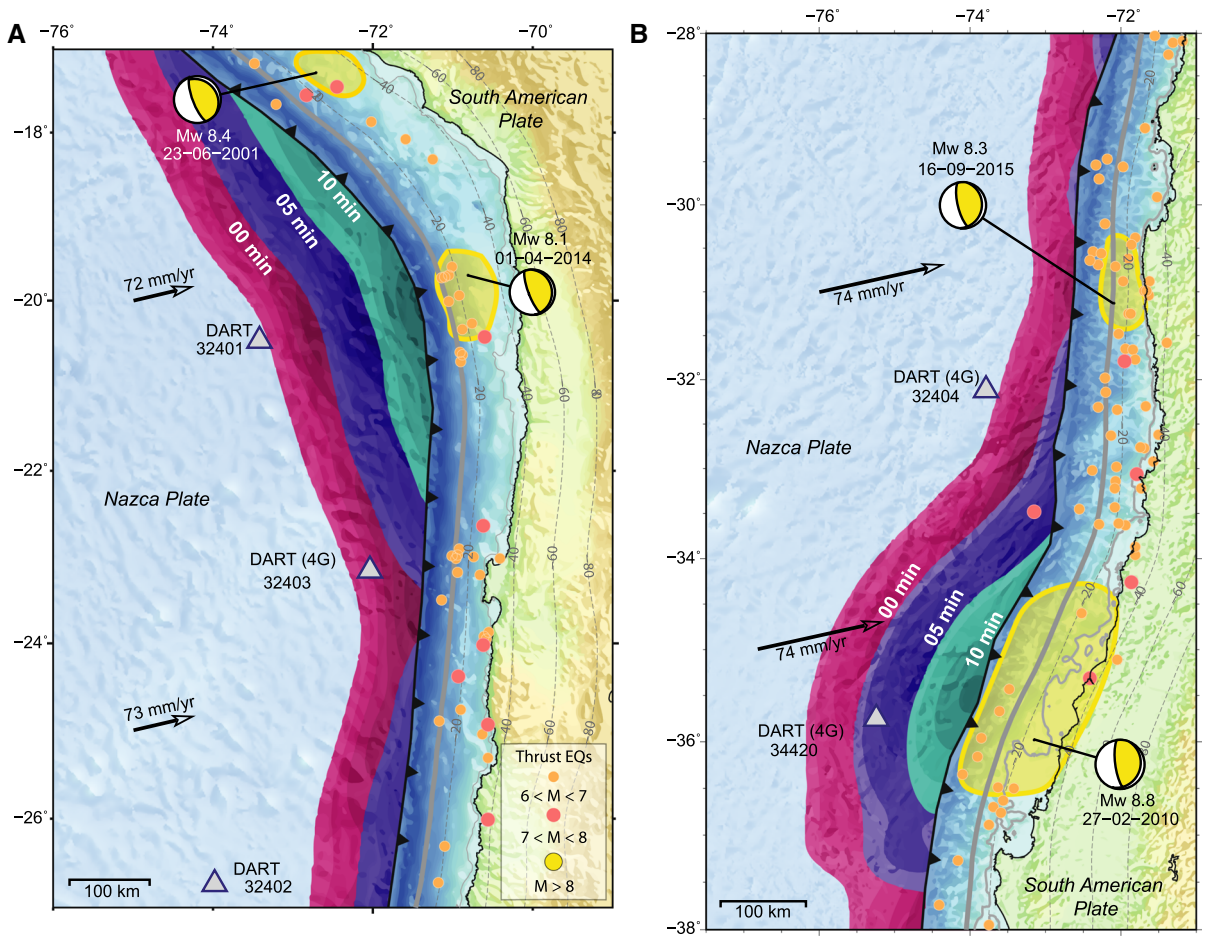

Figure 4

Composite view of northern and central Chile early warning zones. Magenta, navy, and aqua shading refers to 0 min, 5-min, and 10-min lead times, respectively. Arrows indicate the plate motion between the Nazca and South American plates using MORVEL-2010 motions (DeMets et al. 2010) and gray triangles show approximate locations of DART gauges. The thick, gray line that runs trench parallel shows the location of synthetic sources used in the composite. Small dots indicate seismicity recorded in the Harvard CMT catalog over the past 25 years. **a** Northern Peru–Chile trench: yellow polygons show rupture zones from the 23 June 2001 Peru earthquake (Bilek and Ruff 2002) and the 1 April 2014 Iquique earthquake (Lay et al. 2014). **b** Central Peru–Chile trench: yellow polygons show rupture zones from the 27 February 2010 Maule earthquake (Moreno et al. 2010) and 16 September 2015 Illapel earthquake (Williamson et al. 2017)

towards the open ocean and can accommodate a wider region. Localized, near-field tsunami early warning that uses direct tsunami observations in Cascadia are likely limited to this region highlighted in green on Fig. 2. Areas to the south where the shelf tapers do not have the ability for such localized warnings if a rupture were to occur in the immediate vicinity. However, for regional events—such as a Cascadia rupture that is dominantly to the north on the megathrust, the zoning that allows for a feasible tsunami warning system grows substantially.

Three regional DART gauges are included in the composite image to illustrate current operational gauges (DART 46149 and DART 46404) and the DART 4G sensor (DART 46451) which is currently in a testing phase. The 4G gauge's currently deployed location has the ability to offer a larger lead time in warnings along the coast from Washington to Vancouver Island, than conventional DART, aiding in assessment and evacuation efforts. Instrumentation placed further north of DART 46451 in this same trench-proximal locality would be able to not only

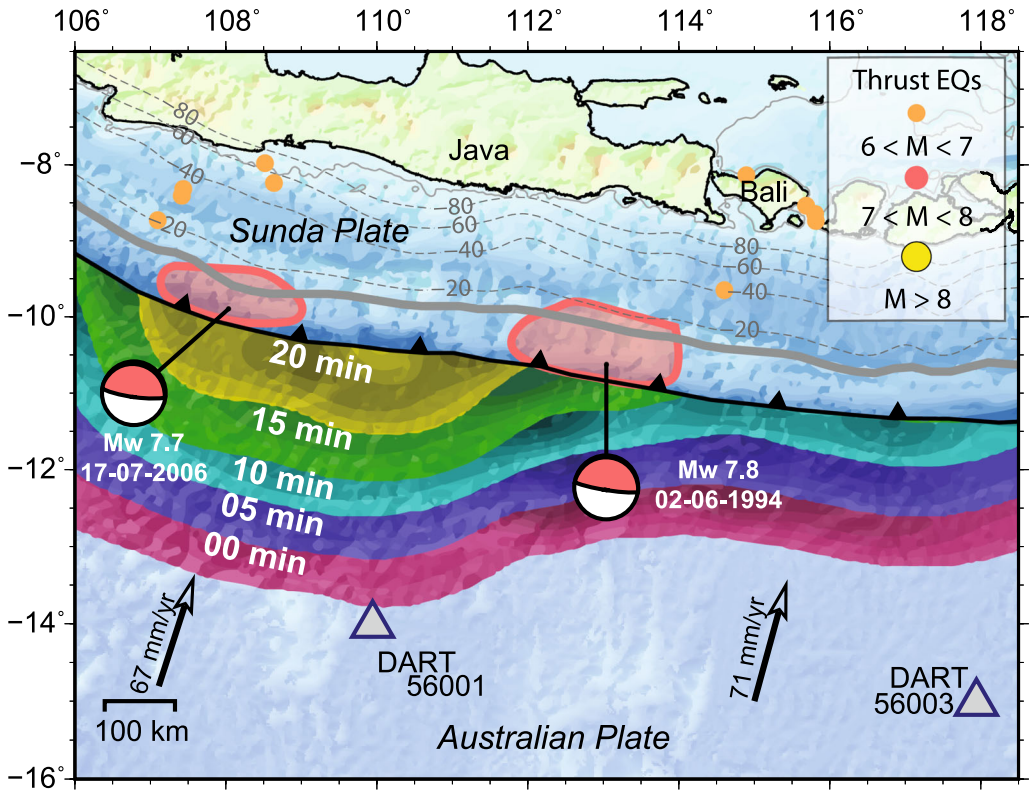

Figure 5

Composite view of Java early warning zones. Magenta, navy, aqua, green, and yellow shading refers to 0 min, 5-min, 10-min, 15-min, and 20-min lead times, respectively. Arrows indicate the plate motion between the Australian and Sunda plates using MORVEL-2010 motions (DeMets et al. 2010) and gray triangles show approximate locations of DART gauges. The thick, gray line that runs trench parallel shows the location of synthetic sources used in the composite. Small dots indicate seismicity recorded in the Harvard CMT catalog over the past 25 years. Pink polygons show the rupture extents from the 2 June 1994 Java tsunami earthquake (Bilek and Engdahl 2007) and the 17 July 2006 Pangandaran tsunami earthquake (Ammon et al. 2006)

provide advanced warning to coastal regions in the Pacific Northwest, but also provide the same mid-and far-field assessments as the older model DART gauges.

In the past decade, the Canadian North-East Pacific Underwater Networked Experiments (NEPTUNE) deployed a cabled network that among other geophysical pursuits, transmits pressure data in real time and can be used for tsunami forecasting (Barnes et al. 2013; Rabinovich and Eblé 2015). The network sits on the accretionary prism offshore from Vancouver Island and provides an intermediate dataset between open-ocean sensors and coastal tide gauges. This network was tested as it recorded the passing of the tsunami generated from the 30 September 2009 Samoa earthquake (M_w 8.1) as it propagated towards the coast of the Pacific Northwest (Thomson et al. 2011). This additional cabled dataset provides useful near-field information that could be integrated into a local tsunami early warning program outside of the DART framework particularly for events affecting the northern portion of the subduction zone.

4.2. *Japan*

Japan has a strong tradition of tsunami research and hazard resilience, built through centuries of observing local and distantly generated tsunami. The linkage between strong shaking from an earthquake and coastal evacuation from an expected tsunami led to the creation of Japan's first tsunami warning center in 1941 (Bernard and Titov 2015). This first center in

Sendai detected earthquakes to determine if evacuation was necessary in nearby coastal cities. The program was later expanded to all of Japan in 1952 (Bernard and Titov 2015). In addition to more characteristic megathrust earthquakes, the Japan trench has also hosted at least one tsunami earthquake in its past. The 1896 Sanriku tsunami earthquake caused extensive casualties due to a lack of perceived shaking on land (Kanamori 1972). The tsunami had estimates of 25–38 m of run-up despite a surface wave-magnitude estimated at 7.0 (Tanioka and Sataka 1996; Mori et al. 2011).

Japan's tsunami warning program was put to test on March 11, 2011 during the devastating Tohoku-Oki earthquake and tsunami. The M_w 9.0 earthquake, rupturing at 14:46:24 local time was initially assessed as a M_w 7.9 (Ozaki 2011; Tang et al. 2012). The Japanese Meteorological Agency (JMA) promptly issued a tsunami warning for nearby prefectures 3 min after the earthquake commenced. Then, W-phase estimates conducted by JMA 20 min after the event's onset confirmed that the earthquake was much larger-closer to a 9.0 (Ritsema et al. 2012). However, the first tsunami models of the event were not available during the initial tsunami warning, but rather were created an hour after the fact, once the tsunami reached the nearest open-ocean gauge (Wei et al. 2014). By this point, the first waves had already reached the coast and additional tsunami information was then put forth for tsunami forecasts for Hawaii and the far-field. It is also important to note this was the first tsunami to be modeled in real time for its far-field inundation hazard (Titov et al. 2016b) through the Pacific Tsunami Warning System. The possible lead times achieved with the data present in 2011 as well as more recent datasets are shown in Fig. S1.

After the 2011 tsunami, three DART gauges were temporarily deployed off the coast of Japan. The more recent, but smaller 2012 M_w 7.3 Japan earthquake and tsunami benefited from the proximal DART gauges sitting closer to the trench, allowing for a shorter time between generation and observation (Bernard et al. 2014). While those three DART sensors have now been removed, a cabled network of 154 seafloor pressure gauges, called S-net, spanning the overriding plate has been completed (Baba et al. 2014; Rabinovich and Eblé 2015). This network's aim is to provide real-time pressure measurements to aid in tsunami warning. Another set of cabled networks, the Dense Ocean-floor Networks for Earthquakes and Tsunamis (DONET-1 and DONET-2) provide pressure gauges and seismometers on the overriding plate, and aid in real-time tsunami detection and observation along the Nankai seismic zone (Baba et al. 2014; Rabinovich and Eblé 2015). Combined, these networks have the possibility of capturing deformation and tsunami generation from locally sourced earthquakes.

Taking into account the density of pressure gauges on the overriding plate as well as nearby DART gauges, the Japan trench provides one of the best locations for the implementation of an early warning system, as shown in Fig. 3. Nowhere else in the world has a network that approaches their offshore instrument density. Japan is already poised to provide rapid direct tsunami observations, possibly aiding in future event forecasts. Additionally, Japan's large distance between trench and coast (100–200 km) along most of the Pacific-Eurasian plate interface facilitates a greater area of potential site locations on the subducting plate than other regions. Even along some parts of the subduction zone, where the trench to shoreline distance is narrower, the presence of a shallow and expansive continental shelf can also effectively slow the oncoming wave, allowing for effective open-ocean instrumentation.

One of the best examples of this is near the Chiba peninsula, east of Tokyo, shown in Fig. 3. The yellow shaded region offshore indicates the instrumentation zone for up to 20 min of lead time before inundation. The strong shelf south of Sendai also acts to curtail the tsunami wave. As a contrast, the tapering and disappearance of the shelf north of Sendai near Miyako leads to slightly less lead time, about 15 min. Along the entire strike of the trench from Chiba peninsula to Hokkaido, a 10- to 15-min lead time is possible. The presence of a dense cabled network also allows for an earlier recording of the tsunami than can be achieved through instruments on the subducting plate, east of the trench. We highlight the warning times achieved for cabled networks on the overriding plate in Fig. S2.

4.3. Peru–Chile

Of the regions analyzed in this study, the Peru–Chile trench is the least feasible for near-field early warning of this type. The region has a relatively fast plate convergence and a history of great ($M_w > 8$) tsunamigenic earthquakes. The 1960 Valdivia earthquake and tsunami originating off the coast of Southern Chile is the largest instrumentally recorded earthquake (M_w 9.5) generating a trans-oceanic tsunami with local maximum run-up heights ranging from 10 to 25 m (NGDC 2017). Within the 1960 rupture zone was the 2016 M_w 7.7 Chiloé earthquake (Ruiz et al. 2017; Moreno et al. 2018). Additional contemporary earthquakes include the 2010 M_w 8.8 Maule earthquake and the 2014 M_w 8.1 Iquique earthquake, both of which generated tsunami. The most recent addition to the Peru–Chile trench sequence is the 2015 M_w 8.3 Illapel earthquake and tsunami. All three of these recent events have included open-ocean DART derived waveforms in conjunction with seismic and/or geodetic observations for detailed analysis of the fault slip post-event, either through time series inversion (Yue et al. 2014; Gusman et al. 2015; Williamson et al. 2017) or forward tsunami modeling for model validation (Heidarzadeh et al. 2016; Li et al. 2016). However, the capability of real-time near-field modeling has not yet been explored in great detail.

Near-field instrumentation feasibility for this region is displayed in Fig. 4. Unlike Cascadia and Japan, the average distance between trench and coastline is small at under 75 km. This shortens the response time before inundation as it places the shallow seismic interface close to shore. The linear coastal morphology with limited and narrow continental shelves does not slow the coastal tsunami propagation as it does elsewhere. Most of the trench only has 5 min or less in lead time, which exceptions near the bend in the subduction zone around the rupture area near the Iquique tsunami, and further south in the former Maule rupture area. This makes most of the region prohibitive of open-ocean early-warning. However, the narrow submarine zone means this area is more advantageous for the inclusion of geodetic datasets to aid in early warning.

The Chilean agency that oversees tsunami data and warnings, the Hydrographic and Oceanic Service of the Chilean Navy (SHOA), has deployed three DART 4G gauges in the near-trench environment. The southernmost gauge, DART 34420, is within a 5-min warning range; however, the gauge immediately to the north (DART 32404), placed just south of the Illapel rupture zone is in the 0-min warning zone. The third gauge, located just south of the Iquique rupture zone, while close to the trench, is also just out of range. It is important to note that these three new sensors, even if not currently suited for direct near-field warning, will provide more open ocean tsunami observations along the strike of the Peru–Chile trench. Before their emplacement, the entire region was served by three older DART sensors (DARTs 32402, 32401, and 32412) located in northern Chile and more distal sensors near Ecuador and Central America. The inclusion of this new dataset, while not ideal for near-field community warnings, could be instrumental in warnings along Chile's extensive coastline outside of the near-field range. The array of DART gauges also provides a useful dataset for far-field warnings affecting Australia and New Zealand.

4.4. Java-Bali, Indonesia

Acting as a catalyst for a global approach to tsunami awareness and forecasting, the 2004 Sumatra earthquake illuminated the possibility of large megathrust earthquakes and tsunami generated in the Indian Ocean basin. Additional $M > 8$ earthquakes have continued to rupture along the southern extent of Sumatra in the years following the 2004 Boxing Day event. Despite their large magnitude, not every large earthquake in the region has generated a hazardous tsunami, making warnings more difficult. Examples include the 2005 Nias earthquake (M_w 8.6). This event, while generating a tsunami that did damage some coastal communities, did not bring the impact that would have been expected of an earthquake rupturing in this region—given the recent 2004 Boxing day earthquake (Song 2007; Borrero et al. 2011). The distinction between hazardous and non-hazardous activity can be difficult to quickly determine remotely without a direct observation. In addition to being a tectonically active and complex

region, half of Indonesia's population resides on the island of Java. The region surrounding Java has not had a great megathrust rupture in recent history but it has had smaller, damaging tsunami earthquakes.

The 1994 Java tsunami earthquake (M_w 7.6) killed over 250 people and was the first thrust mechanism earthquake listed along that region of the Java subduction zone (Abercrombie et al. 2001). It occurred between 16 and 20 km depth (highlighted in Fig. 5) at a far distance from the shoreline. The more recent 2006 Pangandaran tsunami earthquake (M_w 7.8) killed over 600 people. It was particularly deadly because the earthquake was not well felt on land, limiting the reaction time for communities to evacuate from the coastline (Fritz et al. 2007; Ammon et al. 2006). Both events are rarities—the region produces a high number of normal faulting earthquakes which were less productive in generating tsunami (however, tsunami can be generated from normal faulting events). However, the uncommon occurrence of large thrust events—particularly tsunamigenic events, may give communities a false sense of security up until the next earthquake hits.

The region spanning westward from Java towards Bali poses a difficult challenge for some early warning methodologies. The distance from possible shallow source to land-based receivers is high (> 200 km) and the dip of the subducting plate is steep enough that the entirety of the expected seismogenic zone sits offshore, with megathrust interface depths under land reaching upwards of 80 km. This distance poses a far more difficult challenge when using static geodetic (GPS, InSAR) datasets to resolve deformation and tsunami threat than when compared to other regions, such as the Peru–Chile trench. However, this large distance also increases the travel time between source and shoreline for shallow events making it an excellent candidate for tsunami early warning. The region offshore of Pangandaran, just east of the 1996 tsunami earthquake has the opportunity for a near-field tsunami warning system that could be fortuitous for central Java. Synthetic unit sources in this region line-up well with past tsunami earthquakes (Fig. 5). Within central Java, open-ocean datasets could allow for up to 15–20 min of lead time. The main factor that allows for tsunami early warning to be more feasible along central Java and less feasible further east towards Bali is the increase in continental shelf width near Pangandaran. The absence of shallow coastal structures offshore Bali and the rest of the Lesser Sunda Islands increases tsunami arrival time in comparison. Current instrumentation is limited to two Australian owned DART stations (DART 56001 and 56003). These gauges are located too far to be effective for Indonesian early warning.

Unlike other regions examined in this study where the eventual open-ocean propagation of the tsunami remains unhindered for thousands of kilometers, a near-field tsunami warning system for this region adds additional information that can be used to issue warnings for the nearby northwestern shores of Australia. In the event of a larger tsunami stemming from a large Sumatra-style megathrust earthquake, additional infrastructure beyond Australia's two local DART gauges could provide a quicker initial assessment for the country's northern coastline.

5. *Discussion*

Because the location and structure of the next big earthquake is unknown, global models used for assessing tsunami hazard always need to take into account what model assumptions are made. In this paper, two of the biggest assumptions are in the synthetic event source location and the amount of data that can be efficiently incorporated. We also track the crest of the unit source's tsunami wave, both towards the open-ocean and the coast, which at what is expected as peak inundation (excluding reflection), instead of initial inundation. Of these assumptions, the tsunami source location has the largest effect on tsunami travel time and thus the results presented. One end member scenario for tsunami early warning is an event rupturing proximal to the coastline with an immediate or close to immediate inundation. The other end member (for megathrust events) is a near-trench rupture typical of tsunami earthquakes. Rather than make a judgement call on the potential future tsunamigenic sources for each of our study zones, we adopted a streamlined approach of placing all of our sources at the 15 km depth contour of the subducting slab's assumed geometry. While some may argue that

a particular region usually ruptures in a certain location, the earthquake catalog of large megathrust events is not so well defined in any given area that we can definitively point to a local characteristic earthquake that can be confidently used for modeling future hazard. Our general assumed events allow us to focus on the early-warning potential for the region of the megathrust that has a high tsunami hazard. The near-trench environment is also less likely to be resolved form coastal geodetic datasets due to the large distance, lending to the threat of misestimates of tsunami hazard in special tsunami earthquake cases.

We recognize that not all tsunamigenic events occur on the megathrust. Our general source location used for all our regional models also is placed in a way that we can extrapolate the effect of splay faulting on the fore-arc by focusing less on the features any particular faulting pattern and more on the tsunami travel time for a simple disturbed water column. However, steeply dipping splay faults, if activated, have the potential to contribute to large amounts of vertical deformation of the seafloor as has been extrapolated for the Nankai trough (Moore et al. 2007). Splay faults of this nature, located in the accretionary wedge, have also been identified along the Cascadia subduction zone although their future activity is difficult to constrain (Geist and Yoshioka 1996). Tsunami generated on the outer-rise, while also less common, poses a threat for tsunami warning. Recent outer-rise events include 2007 Kuril M_w 8.1 event (Fujii and Satake 2008; Rabinovich et al. 2008). The greater distance between outer rise sources and most coastlines when compared to megathrust events means an extended time before inundation is likely. This should facilitate some of the greatest lead times possible for early warning. Other sources not considered in this work include non-seismically generated tsunamis—the most common of which are landslide-generated tsunamis. Without a strong seismic signature or magnitude to relate to, landslide-generated tsunamis require a direct tsunami observation for an effective tsunami warning.

A second important factor to consider for early-warning feasibility is the timely assimilation of observed data into forecast models. This is dependent on how much data are used. In this study we use the first one-quarter of a tsunami waveform as our threshold for data incorporation. While this is a smaller amount of data than what is currently used to forecast tsunami warnings, the extra error associated with less data is at the trade-off of a quicker warning to affected communities when time is a restricting factor. The use of one-quarter wave periods was assessed for the 2015 Illapel, Chile tsunami with the goal of determining the minimum quantity of open-ocean data required for the earliest possible accurate tsunami forecast (Tang et al. 2016). In this study, the use of the first one-quarter of the recorded waveform was effectively inverted to determine a source model that could be applied for near-field early warning forecasts. This is an abbreviation of the half-wave model (Titov et al. 2016b), which can also be used and yields a slight improvement to fit. The full-wave inversion provides additional unique information, but only a marginally better forecast at the expense of a longer wait time between source and final recording.

The amount of data used in a rapid inversion also affects the processing required. When handling data derived from the open-ocean, tidal signals need to be removed to provide a meaningful dataset. The uncertainty involved in de-tiding datasets should be low enough that a reasonable forecast can still be made. In Percival et al. (2015), the de-tiding of tsunami signals is assessed with synthetic data to view the degree of error from using different filtering methods as well as differing quantities of data. An important takeaway from the study is that while the best results are attained by using over one full wavelength of data, methodologies that incorporated only one-quarter of the wavelength did as sufficient of a job at resolving the unknown slip parameters as half- and three-quarter wavelength solutions. While, like Tang et al. (2016) showed, the best possible solutions are attained with the most data, the increased time needed did not substantially change the final results. In terms of early warning, a slight change in the forecast solution at the cost of tens of minutes of warning time may not always be substantiated.

An additional factor that has been omitted from the work thus far is commentary on the cost of deploying new instrumentation in the open-ocean. The deployment and maintenance on any instrument, including ship-time for servicing can be substantial.

We do not focus on the deployment logistics of adding new stations further as it is outside the scope of this paper. As mentioned in Bernard and Titov (2015) approximated costs of new DART stations can reach $0.5 million per station. Cabled observatories, like those found in Japan have a starting cost of $500 million for the entire network. We do note that by focusing on which regions can facilitate early-warnings, we can reduce the total number of stations that would need to be deployed to be as cost-effective as possible.

6. Conclusion

Through this study, we explore four regions to examine where a localized near-field tsunami system would be effective. Ideally this system would incorporate near-trench, open-ocean, tsunami observations, through pressure gauges such as the currently deployed DART system or through cabled pressure stations. The advantages of direct tsunami measurements over seismic and geodetically focused approaches are listed below. First, tsunami datasets do not rely on the accuracy of an earthquake magnitude. This can be particularly important for tsunami earthquakes and large earthquakes with long rupture durations. Second, tsunami-based models do not need to understand the relationship between the transfer of earthquake energy to tsunami energy. This is crucial, because estimates in earthquake energy can vary greatly in the first hour after rupture and so little of that energy (0.1%) is transferred to the ocean (Titov et al. 2016a). Third, tsunami-based models can directly observe the oncoming threat for forecasting purposes without making assumptions on the fault geometry. Fourth, tsunami-based models can incorporate non-seismic contributions to the tsunami wave such as submarine mass failures. As Bernard and Titov (2015) have noted—20% of tsunamis are generated from non-seismic sources.

The main limitation to this direct observation approach is having enough instrumentation to cover high-risk areas near the trench. This is both a resource and financial limitation. If newer DART systems or comparable open-ocean datasets prove robust and yield fruitful tsunami information despite strong shaking from the earthquake, regions like the Cascadia subduction zone are viable for near-field tsunami warning. Other regions, such as proximal to Java, Indonesia, do not have the near-field infrastructure but could benefit from an early warning of this variety—particularly due to their contemporary history of tsunami earthquakes. Chile, while having near-trench open-ocean tsunami data, is poorly suited for local early warning, given its subducting fault geometry and prohibitive continental shelf geometry. However, those observations are still useful for mid-field warnings within the Peru–Chile trench. Based on this study, our primary findings are that while some regions are ill-suited for this type of early warning, other localities could incorporate direct tsunami observations into their hazard forecasts with enough lead time to be effective for coastal community emergency response. Particular coastal areas with associated high potential tsunami lead times could have a localized system which may require only one to two open-ocean stations.

We do not advocate to dismantle or delay current tsunami warnings and advisories already in place and rooted in public knowledge for coastal communities. However, the vast majority of potential tsunami victims are located in the near-field coastal areas. Improvements on near-field tsunami warnings can save lives (Titov et al. 2016a). The inclusion of additional tsunami data can create an added push for further evacuation if needed in the case of underestimations of the perceived hazard. It can also add confidence to accurate warnings already in place and act as an additional dataset for mid- and far-field forecasts.

Acknowledgements

This research was supported through State Funds through Georgia Tech to AVN. Figures were generated using Generic Mapping Tools from Wessel et al. (2013). Training on usage and implementation of the MOST tsunami model was made possible through the assistance of V. Titov, D. Arcas, and Y. Wei at the Pacific Marine Environmental Laboratory.

References

Abercrombie, R. E., Antolik, M., Felzer, K., & Ekström, G. (2001). The 1994 Java tsunami earthquake: Slip over a subducting seamount. *Journal of Geophysical Research: Solid Earth, 106*(B4), 6595–6607. https://doi.org/10.1029/2000JB900403.

Ammon, C. J., Kanamori, H., Lay, T., & Velasco, A. A. (2006). The 17 July 2006 Java tsunami earthquake. *Geophysical Research Letters*. https://doi.org/10.1029/2006GL028005.

Atwater, B. F. (1992). Geologic evidence for earthquakes during the past 2000 years along the Copalis River, southern coastal Washington. *Journal of Geophysical Research: Solid Earth, 97*(B2), 1901–1919. https://doi.org/10.1029/91JB02346.

Baba, T., Takahashi, N., & Kaneda, Y. (2014). Near-field tsunami amplification factors in the Kii Peninsula, Japan for Dense Oceanfloor Network for Earthquakes and Tsunamis (DONET). *Marine Geophysical Research, 35*(3), 319–325. https://doi.org/10.1007/s11001-013-9189-1.

Barnes, C. R., Best, M. M., Johnson, F. R., Pautet, L., & Pirenne, B. (2013). Challenges, benefits, and opportunities in installing and operating cabled ocean observatories: Perspectives from NEPTUNE Canada. *IEEE Journal of Oceanic Engineering, 38*(1), 144–157.

Bernard, E. N., & Titov, V. V. (2015). Evolution of tsunami warning systems and products. *Philosophical Transactions of the Royal Society A, 373*(2053), 20140371.

Bernard, E. N., Wei, Y., Tang, L., & Titov, V. V. (2014). Impact of near-field, deep-ocean tsunami observations on forecasting the 7 December 2012 Japanese tsunami. *Pure and Applied Geophysics, 171*(12), 3483–3491. https://doi.org/10.1007/s00024-013-0720-8.

Bilek, S. L., & Engdahl, E. R. (2007). Rupture characterization and aftershock relocations for the 1994 and 2006 tsunami earthquakes in the Java subduction zone. *Geophysical Research Letters, 34,* L20311. https://doi.org/10.1029/2007GL031357.

Bilek, S. L., & Ruff, L. J. (2002). Analysis of the 23 June 2001 M_w = 8.4 Peru underthrusting earthquake and its aftershocks. *Geophysical Research Letters, 29*(20), 1960. https://doi.org/10.1029/2002GL015543.

Borrero, J. C., McAdoo, B., Jaffe, B., Dengler, L., Gelfenbaum, G., Higman, B., et al. (2011). Field survey of the March 28, 2005 Nias-Simeulue earthquake and tsunami. *Pure and Applied Geophysics, 168*(6–7), 1075–1088.

DeMets, C., Gordon, R. G., & Argus, D. F. (2010). Geologically current plate motions. *Geophysical Journal International, 181*(1), 1–80. https://doi.org/10.1111/j.1365-246X.2009.04491.x.

Fritz, H. M., Kongko, W., Moore, A., McAdoo, B., Goff, J., Harbitz, C., et al. (2007). Extreme runup from the 17 July 2006 Java tsunami. *Geophysical Research Letters*. https://doi.org/10.1029/2007GL029404.

Fujii, Y., & Satake, K. (2008). Tsunami sources of the November 2006 and January 2007 great Kuril earthquakes. *Bulletin of the Seismological Society of America, 98*(3), 1559–1571.

Geist, E., & Yoshioka, S. (1996). Source parameters controlling the generation and propagation of potential local tsunamis along the Cascadia margin. *Natural Hazards, 13*(2), 151–177.

Gusman, A. R., Murotani, S., Satake, K., Heidarzadeh, M., Gunawan, E., Watada, S., et al. (2015). Fault slip distribution of the 2014 Iquique. *Chile, earthquake estimated from ocean-wide tsunami waveforms and GPS data, Geophysical Research Letters, 42*(4), 1053–1060. https://doi.org/10.1002/2014gl062604.

Gusman, A. R., Tanioka, Y., Sakai, S., & Tsushima, H. (2012). Source model of the great 2011 Tohoku earthquake estimated from tsunami waveforms and crustal deformation data. *Earth and Planetary Science Letters, 341,* 234–242.

Hayes, G. P., Wald, D. J., & Johnson, R. L. (2012). Slab1.0: A three-dimensional model of global subduction zone geometries. *Journal of Geophysical Research, 117,* B01302. https://doi.org/10.1029/2011JB008524.

Heidarzadeh, M., Murotani, S., Satake, K., Ishibe, T., & Gusman, A. R. (2016). Source model of the 16 September 2015 Illapel, Chile, M_w 8.4 earthquake based on teleseismic and tsunami data. *Geophysical Research Letters, 43,* 643–650. https://doi.org/10.1002/2015GL067297.

Hossen, M. J., Cummins, P. R., Dettmer, J., & Baba, T. (2015). Time reverse imaging for far-field tsunami forecasting: 2011 Tohoku earthquake case study. *Geophysical Research Letters, 42,* 9906–9915. https://doi.org/10.1002/2015GL065868.

Kanamori, H. (1972). Mechanism of tsunami earthquakes. *Physics of the Earth and Planetary Interiors, 6*(5), 346–359. https://doi.org/10.1016/0031-9201(72)90058-1.

Kanamori, H., & Kikuchi, M. (1993). The 1992 Nicaragua earthquake: A slow tsunami earthquake associated with subducted sediments. *Nature, 361*(6414), 714–716. https://doi.org/10.1038/361714a0.

Lay, T. (2015). The surge of great earthquakes from 2004 to 2014. *Earth and Planetary Science Letters, 409,* 133–146. https://doi.org/10.1016/j.epsl.2014.10.047.

Lay, T., Yue, H., Brodsky, E. E., & An, C. (2014). The 1 April 2014 Iquique, Chile, M_w 8.1 earthquake rupture sequence. *Geophysical Research Letters, 41,* 3818–3825. https://doi.org/10.1002/2014GL060238.

Li, L., Lay, T., Cheung, K. F., & Ye, L. (2016). Joint modeling of teleseismic and tsunami wave observations to constrain the 16 September 2015 Illapel, Chile, Mw 8.3 earthquake rupture process. *Geophysical Research Letters, 43,* 4303–4312. https://doi.org/10.1002/2016GL068674.

Melgar, D., LeVeque, R. J., Dreger, D. S., & Allen, R. M. (2016). Kinematic rupture scenarios and synthetic displacement data: An example application to the Cascadia subduction zone. *Journal of Geophysical Research: Solid Earth, 121*(9), 6658–6674.

Moore, G. F., Bangs, N. L., Taira, A., Kuramoto, S., Pangborn, E., & Tobin, H. J. (2007). Three-dimensional splay fault geometry and implications for tsunami generation. *Science, 318*(5853), 1128–1131.

Moreno, M., Li, S., Melnick, D., Bedford, J. R., Baez, J. C., Motagh, M., et al. (2018). Chilean megathrust earthquake recurrence linked to frictional contrast at depth. *Nature Geoscience, 11,* 285.

Moreno, M., Rosenau, M., & Oncken, O. (2010). 2010 Maule earthquake slip correlates with pre-seismic locking of Andean subduction zone. *Nature, 467*(7312), 198. https://doi.org/10.1038/nature09349.

Mori, N., Takahashi, T., Yasuda, T., & Yanagisawa, H. (2011). Survey of 2011 Tohoku earthquake tsunami inundation and run-up. *Geophysical Research Letters*. https://doi.org/10.1029/2011GL049210.

National Geophysical Data Center database (NGDC). (2017). https://www.ngdc.noaa.gov. Accessed 19 Sept 17.

Newman, A. V., Hayes, G., Wei, Y., & Convers, J. (2011). The 25 October 2010 Mentawai tsunami earthquake, from real-time discriminants, finite-fault rupture, and tsunami excitation.

Geophysical Research Letters. https://doi.org/10.1029/2010GL046498.

Newman, A. V., & Okal, E. A. (1998). Teleseismic estimates of radiated seismic energy: The E/M 0 discriminant for tsunami earthquakes. *Journal of Geophysical Research: Solid Earth, 103*(B11), 26885–26898. https://doi.org/10.1029/98jb02236.

Okal, E. A. (2015). The quest for wisdom: Lessons from 17 tsunamis, 2004–2014. *Philosophical Transactions of the Royal Society A, 373*(2053), 20140370. https://doi.org/10.1098/rsta.2014.0370.

Ozaki, T. (2011). Outline of the 2011 off the Pacific coast of Tohoku Earthquake (M_w 9.0). *Earth, Planets and Space, 63*(7), 57.

Percival, D. B., Denbo, D. W., Eblé, M. C., Gica, E., Huang, P. Y., Mofjeld, H. O., et al. (2015). Detiding DART® buoy data for real-time extraction of source coefficients for operational tsunami forecasting. *Pure and Applied Geophysics, 172*(6), 1653–1678.

Polet, J., & Kanamori, H. (2000). Shallow subduction zone earthquakes and their tsunamigenic potential. *Geophysical Journal International, 142*(3), 684–702. https://doi.org/10.1046/j.1365-246x.2000.00205.x.

Rabinovich, A. B., & Eblé, M. C. (2015). Deep-ocean measurements of tsunami waves. *Pure and Applied Geophysics, 172*(12), 3281–3312.

Rabinovich, A. B., Lobkovsky, L. I., Fine, I. V., Thomson, R. E., Ivelskaya, T. N., & Kulikov, E. A. (2008). Near-source observations and modeling of the Kuril Islands tsunamis of 15 November 2006 and 13 January 2007. *Advances in Geosciences, 14,* 105–116.

Ritsema, J., Lay, T., & Kanamori, H. (2012). The 2011 Tohoku Earthquake. *Elements, 8*(3), 183–188.

Rogers, G., & Dragert, H. (2003). Episodic tremor and slip on the Cascadia subduction zone: The chatter of silent slip. *Science, 300*(5627), 1942–1943. https://doi.org/10.1126/science.1084783.

Ruiz, S., Moreno, M., Melnick, D., Campo, F., Poli, P., Baez, J. C., Leyton F., & Madariaga, R. (2017). Reawakening of large earthquakes in South-Central Chile: The 2016 M_w 7.6 Chiloé event. *Geophysical Research Letters*. *44*(13), 6633–6640.

Satake, K., Shimazaki, K., Tsuji, Y., & Ueda, K. (1996). Time and size of a giant earthquake in Cascadia inferred from Japanese tsunami records of January 1700. *Nature, 379*(6562), 246–249. https://doi.org/10.1038/379246a0.

Satake, K., Wang, K., & Atwater, B. F. (2003). Fault slip and seismic moment of the 1700 Cascadia earthquake inferred from Japanese tsunami descriptions. *Journal of Geophysical Research: Solid Earth*. https://doi.org/10.1029/2003JB002521.

Song, Y. T. (2007). Detecting tsunami genesis and scales directly from coastal GPS stations. *Geophysical Research Letters*. https://doi.org/10.1029/2007GL031681.

Tang, L., Titov, V. V., Bernard, E. N., Wei, Y., Chamberlin, C. D., & Newman, J. C., et al. (2012). Direct energy estimation of the 2011 Japan tsunami using deep-ocean pressure measurements. *Journal of Geophysical Research: Oceans, 117*(C8), C08008.

Tang, L., Titov, V. V., Moore, C., & Wei, Y. (2016). Real-time assessment of the 16 September 2015 Chile tsunami and implications for near-field forecast. *Pure and Applied Geophysics, 173*(2), 369–387.

Tanioka, Y., & Sataka, K. (1996). Fault parameters of the 1896 Sanriku tsunami earthquake estimated from tsunami numerical modeling. *Geophysical Research Letters, 23*(13), 1549–1552. https://doi.org/10.1029/96gl01479.

Thomson, R., Fine, I., Rabinovich, A., Mihály, S., Davis, E., Heesemann, M., et al. (2011). Observation of the 2009 Samoa tsunami by the NEPTUNE-Canada cabled observatory: Test data for an operational regional tsunami forecast model. *Geophysical Research Letters, 38,* L11701. https://doi.org/10.1029/2011GL046728.

Titov, V.V., & González F.I. (1997). Implementation and testing of the method of splitting tsunami (MOST) model. US Department of Commerce, National Oceanic and Atmospheric Administration, Environmental Research Laboratories, Pacific Marine Environmental Laboratory.

Titov, V.V., Kânoğlu U., & Synolakis C. (2016b). *Development of MOST for real-time tsunami forecasting*. Diss. American Society of Civil Engineers. https://doi.org/10.1061/(asce)ww.1943-5460.000035703116004.

Titov, V., Rabinovich, A. B., Mofjeld, H. O., Thomson, R. E., & González, F. I. (2005). The global reach of the 26 December 2004 Sumatra tsunami. *Science, 309*(5743), 2045–2048.

Titov, V. V., Song, Y. T., Tang, L., Bernard, E. N., Bar-Sever, Y., & Wei, Y. (2016). Consistent estimates of tsunami energy show promise for improved early warning. *Pure and Applied Geophysics, 173*(12), 3863–3880. https://doi.org/10.1007/s00024-016-1312-1.

Wei, Y., Newman, A. V., Hayes, G. P., Titov, V. V., & Tang, L. (2014). Tsunami forecast by joint inversion of real-time tsunami waveforms and seismic or GPS data: Application to the Tohoku 2011 tsunami. *Pure and Applied Geophysics, 171*(12), 3281–3305. https://doi.org/10.1007/s00024-014-0777-z.

Wessel, P., Smith, W. H. F., Scharroo, R., Luis, J. F., & Wobbe, F. (2013). Generic Mapping Tools: Improved version released. *EOS Trans AGU, 94,* 409–410.

Williamson, A., Newman, A. V., & Cummins, P. R. (2017). Reconstruction of coseismic slip from the 2015 Illapel earthquake using combined geodetic and tsunami waveform data. *Journal of Geophysical Research: Solid Earth, 122*(3), 2119–2130. https://doi.org/10.1002/2016jb013883.

Witter, R. C., Zhang, Y. J., Wang, K., Priest, G. R., Goldfinger, C., Stimely, L., et al. (2013). Simulated tsunami inundation for a range of Cascadia megathrust earthquake scenarios at Bandon, Oregon, USA. *Geosphere, 9*(6), 1783–1803.

Yue, H., Lay, T., Rivera, L., An, C., Vigny, C., Tong, X., et al. (2014). Localized fault slip to the trench in the 2010 Maule, Chile M_w = 8.8 earthquake from joint inversion of high-rate GPS, teleseismic body waves, InSAR, campaign GPS, and tsunami observations. *Journal of Geophysical Research: Solid Earth, 119*(10), 7786–7804. https://doi.org/10.1002/2014jb011340.

(Received October 25, 2017, revised May 2, 2018, accepted May 4, 2018)